LASER & PHOTONICS REVIEWS

www.lpr-journal.org

Temperature-dependent magneto-photoluminescence spectroscopy of carbon nanotubes: evidence for dark excitons

Jonah Shaver and **Junichiro Kono**

Department of Electrical and Computer Engineering, Rice University, Houston, Texas 77005, USA

Received 7 August 2007, revised 10 October 2007, accepted 17 October 2007
Published online 16 November 2007

Key words single-walled carbon nanotubes; photoluminescence; excitons; Aharonov-Bohm effect
PACS 78.67.Ch, 71.35.Ji, 78.55.-m

We review recent experimental and theoretical studies on the radiative properties of excitons in single-walled carbon nanotubes (SWNTs) as a function of magnetic field and temperature. These studies not only provide new insight into the fundamental properties of excitons in the ultimate one-dimensional (1D) limit but also reveal new phenomena associated with the unique crystal and electronic structure of SWNTs. During the past several years, SWNTs have emerged as one of the most ideal systems available for the systematic study of 1D excitons, which are predicted to possess a set of properties that are distinctly different from excitons in higher dimensions. In addition, their tubular nature allows them to exhibit non-intuitive quantum phenomena when subjected to a parallel magnetic field, which breaks time reversal symmetry and adds an Aharonov-Bohm phase to the electronic wavefunction. In particular, a series of recent experiments demonstrate that such a symmetry-breaking magnetic field can dramatically "brighten" an optically-inactive, or *dark*, exciton state at low temperature (see the title figure on the right). We show that this phenomenon, *magnetic brightening*, can be understood as a consequence of interplay between the strong intervalley Coulomb mixing and field-induced lifting of valley degeneracy. Detailed temperature-dependent photoluminescence studies of excitons in SWNTs in a varying magnetic field have thus provided one of the most critical tests for recently proposed theories of 1D excitons taking into account the strong 1D Coulomb interactions and unique band structure on an equal footing. Furthermore, results of these studies suggest the intriguing possibility of manipulating the optical properties of SWNTs by judicious symmetry control, which can lead to novel devices and applications in lasers and optoelectronics.

Laser & Photon. Rev. **1**, No. 3, 260 – 274 (2007) / **DOI** 10.1002/lpor.200710018

Laser & Photon. Rev. **1**, No. 3, 260–274 (2007) / **DOI** 10.1002/lpor.200710018

Abstract We review recent experimental and theoretical studies on the radiative properties of excitons in single-walled carbon nanotubes (SWNTs) as a function of magnetic field and temperature. These studies not only provide new insight into the fundamental properties of excitons in the ultimate one-dimensional (1D) limit but also reveal new phenomena associated with the unique crystal and electronic structure of SWNTs. During the past several years, SWNTs have emerged as one of the most ideal systems available for the systematic study of 1D excitons, which are predicted to possess a set of properties that are distinctly different from excitons in higher dimensions. In addition, their tubular nature allows them to exhibit non-intuitive quantum phenomena when subjected to a parallel magnetic field, which breaks time reversal symmetry and adds an Aharonov-Bohm phase to the electronic wavefunction. In particular, a series of recent experiments demonstrate that such a symmetry-breaking magnetic field can dramatically "brighten" an optically-inactive, or *dark*, exciton state at low temperature (see the title figure on the right). We show that this phenomenon, *magnetic brightening*, can be understood as a consequence of interplay between the strong intervalley Coulomb mixing and field-induced lifting of valley degeneracy. Detailed temperature-dependent photoluminescence studies of excitons in SWNTs in a varying magnetic field have thus provided one of the most critical tests for recently proposed theories of 1D excitons taking into account the strong 1D Coulomb interactions and unique band structure on an equal footing. Furthermore, results of these studies suggest the intriguing possibility of manipulating the optical properties of SWNTs by judicious symmetry control, which can lead to novel devices and applications in lasers and optoelectronics.

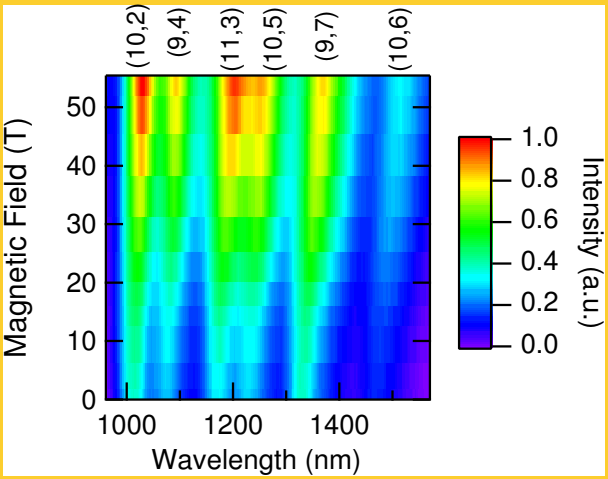

Photoluminescence (excited at 780 nm, 1.59 eV) intensity of a carbon nanotube film vs. magnetic field at 5 K. As the magnetic field is increased, the photoluminescence intensity dramatically increases and the peak positions red-shift. The six excited nanotube species' (n, m) types are indicated.

Temperature-dependent magneto-photoluminescence spectroscopy of carbon nanotubes: evidence for dark excitons

Jonah Shaver and Junichiro Kono[*]

Department of Electrical and Computer Engineering, Rice University, Houston, Texas 77005, USA

Received: 7 August 2007, Revised: 10 October 2007, Accepted: 17 October 2007
Published online: 16 November 2007

Key words: single-walled carbon nanotubes; photoluminescence; excitons; Aharonov-Bohm effect

PACS: 78.67.Ch, 71.35.Ji, 78.55.-m

Corresponding author: e-mail: kono@rice.edu

1. Introduction

Optical properties of one-dimensional (1D) systems have attracted much attention for both applications and basic research for many years. For example, the concentration of carriers at the band edge in a 1D semiconductor is predicted to lead to a high degree of thermal stability and stable lasing properties over a larger temperature range [1]. From a fundamental point of view, the spatial confinement in 1D systems results in interesting excitonic properties. Strong Coulomb interactions among particles in a 1D system are expected to produce excitons that behave very differently from those in higher dimensions. Some of these predictions are a Sommerfeld factor (the ratio of excitonic continuum absorption to the above band edge free carrier absorption) less than 1 [2, 3], infinite binding energy [4–6], stability at high excitation density [7–9], and long intrinsic radiative lifetimes [10]. Radiative decay rates are greatly influenced by the convolution of the density of states and a thermal distribution of excitons [10]. Fig. 1 shows the difference in exciton occupation (density of states multiplied by a Boltzmann distribution) near the band edge in 1, 2, and 3D systems and the resulting temperature (T) dependent radiative decay rates [10, 11].

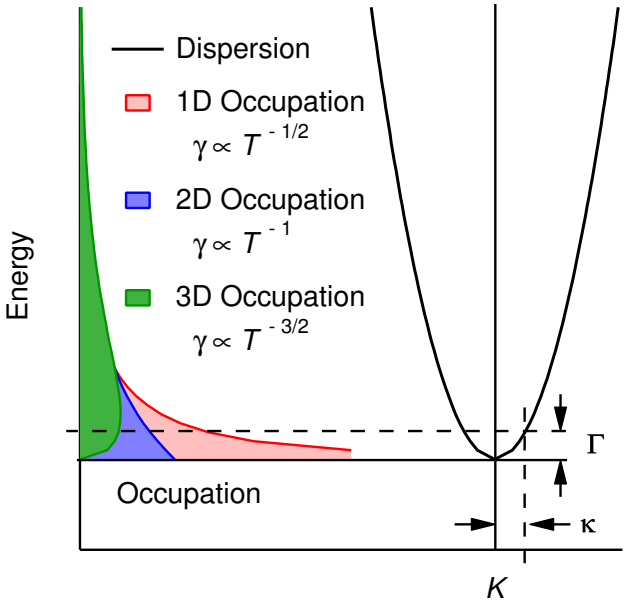

Figure 1 Schematic of thermal population of excitons in systems of different dimensionality (left) together with exciton energy dispersion (right). The occupation (density of states multiplied by a Boltzmann distribution) is plotted vs. energy. Only a small fraction are within the optically allowed region $|K| \leq \kappa$ (corresponding energy of Γ), where K is the wave vector associated with the exciton center-of-mass momentum. As the temperature decreases, the population distribution narrows and concentrates at the bottom of the band. 1D systems have a higher concentration of population at the band edge than both two and three dimensional systems due to the concentrated density of states at the band edge. This difference influences the temperature (T) dependence of the radiative decay rate (γ) in systems of different dimensionality.

Single-walled carbon nanotubes (SWNTs) are one of the most ideal 1D systems available for study. Their small diameters result in a high subband separation and exciton binding energies. Produced by various methods of catalytic carbon decomposition on the surface of ferromagnetic nanoparticles, SWNTs are essentially rolled up sheets of graphene. The optical and electronic properties of these tubes are determined by their physical structure, that is, the precise way the graphene sheet is rolled. Each unique species can be identified by its n and m indices, which are determined by counting the number of unit cells along the edges of a sheet of graphene, 30° apart [12, 13]. These indices define the electronic structure of the nanotube, i.e., $(n-m)$ mod $3 = 0$ for metallic, $(n-m)$ mod $3 = 1$ or 2 for semiconducting.

Due to the strong van der Waals interactions between nanotubes, and efficient quenching mechanisms that result, it was more than 10 years after the first identification of carbon nanotubes [14] until the first observation of photoluminescence [15]. Individualization through surfactant stabilization opened the field of nanotube optics and nanospectroscopy, which has been the focus of intense study in recent years [16, 17]. Photoluminescence excitation spectroscopy enabled the assignment of spectral features to specific (n,m) species [18–21]. Time-resolved optical spectroscopy [22–29] revealed details of decay processes of photo-excited carriers, excitons, and phonons. Various microscopies [30–34] have collected signals from individual nanotubes. Magneto-optical studies [35–39] have begun to reveal details of the excitonic structure.

A standing issue in SWNT optics has been their low photoluminescence quantum yield, that is, only a very small fraction (10^{-3} to 10^{-4}) of absorbed photons are re-emitted in fluorescence while the vast majority seem to decay non-radiatively [15, 24]. Though higher quality samples are being prepared with quantum yields up to $\sim 10^{-2}$ [40–42], the exact source of the low quantum yield is still elusive. Possible sources include Auger recombination at high excitation density [24, 43–45], multi-phonon processes [46, 47], sample purity [48, 49] and optically inactive excitons [50–54]. Optically-inactive, or dark excitons, below the first optically-active exciton state, can trap much of the exciton population at low temperature. This is due to the doubly-degenerate conduction and valence bands of SWNTs as well as the characteristic very strong Coulomb interactions among charge carriers in low-dimensional systems. Recent magneto-optical measurements have conclusively proven the existence of dark excitons in SWNTs [38, 39], as described in Sect. 3.4.

Here, we review current theoretical and experimental progress toward understanding the influence of magnetic field and temperature on photoluminescence intensity and radiative decay mechanisms in SWNTs. In the theory section, we will cover calculations and predictions of the excitonic structure and how it is modified by a mag-

netic field. The temperature dependence of photoluminescence intensity will also be discussed in the absence and presence of a magnetic field. In the experimental section, we will first focus on magnetic-field-dependent photoluminescence at room temperature, proving the predicted effects on the band structure. Second, we will cover the temperature dependence of photoluminescence intensity, showing the influence of the predicted excitonic structure. The third portion, combining magnetic field and temperature dependence, dramatically demonstrates the power of utilizing microscopic-symmetry manipulation in conjunction with exciton population restriction, not only to determine the nature of SWNT excitonic structure, but also to directly control the measurable macroscopic properties of photoluminescence.

2. Theory

2.1. Radiative decay in 1D

To satisfy longitudinal energy-momentum conservation in a 1D system, only excitons with momentum near that of light can decay radiatively. Taking into account a Boltzmann distribution of excitons, Citrin calculated the radiative decay rate in semiconductor quantum wires, finding a $1/\sqrt{T}$ temperature scaling behavior [10]. The decay rate is enhanced by an order of magnitude over 2D and 3D systems due to thermal averaging over the density of states, as explained in Fig. 1. This scaling behavior was observed by Akiyama et al. in 1D quantum wires and compared to 2D quantum wells [11].

In a real system, the energy-momentum conservation requirement is relaxed by phonon scattering and impurity induced disorder, resulting in a finite linewidth, which removes the divergence of the decay rate at very low temperature. Fig. 1 describes the optically active energy region (Γ) that corresponds not to the light dispersion, but to a larger K-vector, defined as κ, due to these scattering mechanisms. An important assumption in this interpretation is that the effective thermalization time is much less than the radiative lifetime. If this condition is not met, a non-thermal distribution of excitons will result and the Boltzmann distribution this analysis is based on will no longer be valid.

2.2. Excitons in SWNTs

As expected, excitonic effects are very important in SWNTs [55–60]. Two-photon photoluminescence excitation measurements by Wang et al. [61] and Maultzsch et al. [62] showed binding energies in the ∼300 meV range for ∼1 nm diameter SWNTs. Nanotubes also have valley degeneracy, that is, there are two equivalent energy conduction and valence bands in k-space in the vicinity of the K and K′ points at the corners of the hexagonal Brillouin

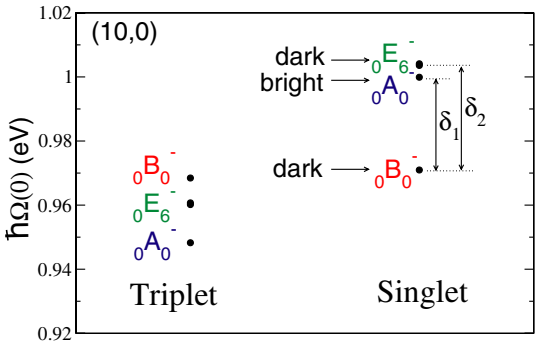

Figure 2 Relative energy of SWNT excitonic levels for the (10,0) nanotube determined by *ab initio* calculations. The highest energy singlet state is two-fold degenerate, while the lower energy triplet states are three-fold degenerate, and the higher energy triplet state is six-fold degenerate. (Reprinted figure with permission from C. D. Spataru, S. Ismail-Beigi, R. B. Capaz, and S. G. Louie [53]. Copyright 2005 by the American Physical Society.)

zone of graphene. Coulomb interactions between carriers in the two k-space valleys influence the energy levels and selection rules of the excitonic transitions.

Theory predicts the existence of optically inactive excitons in SWNTs [50–54]. Four-fold valley degeneracy in combination with four-fold spin degeneracy gives rise to 16 electron-hole pair states in SWNTs. The short-range exchange Coulomb interaction partially lifts the degeneracy of these states. Of the four singlet states, the lowest energy state is even parity and zero angular momentum, and hence optically inactive, or dark. The next exciton is odd parity and zero angular momentum, making it optically active, or bright. The remaining two degenerate, higher energy states have non-zero angular momentum and are also dark (see Fig. 2).

The Coulomb exchange interaction diverges in low dimensions [63, 64] and leads to a logarithmic singularity, $K^2 \log K$, in the bright exciton dispersion [52]. Away from the bottom of the band, the dispersion can be approximated by a hyperbolic dispersion [65]. Fig. 3 plots the dispersions of the zero angular momentum, dark ($i = \delta$), bright ($i = \beta$), and the finite angular momentum, dark ($i = \alpha$), excitons, given by $E_i(K) = \sqrt{\Delta_i^2 + \Delta_i \hbar K^2/m_i}$, for a (9,4) SWNT. Here Δ_i is the energy at the bottom of the i-th band, m_i is the effective mass of the i-th band, and K is the wave vector associated with the exciton center-of-mass momentum.

2.3. Radiative decay in SWNTs

In a photoluminescence experiment on a nanotube without symmetry breaking interactions, excitons can radiatively decay only when they are in an odd parity singlet state. Using the same assumptions as Citrin [10], Spataru et al. [53]

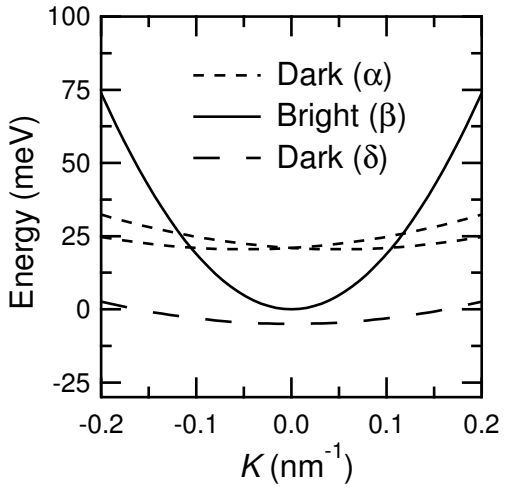

Figure 3 Energy dispersions of the four singlet excitons plotted in relation to the bottom of the bright band for a (9,4) nanotube vs. center-of-mass momentum, calculated based on equations from Perebeinos et al. [52]. Optically active bands are solid lines, and inactive bands are dashed. Two higher energy, finite angular momentum bands (α) are dark and displaced in k-space by $\approx \pm 0.05\,\mathrm{nm}^{-1}$ from $K = 0$. The zero angular momentum states of even (δ) and odd (β) parity are dark and bright, respectively.

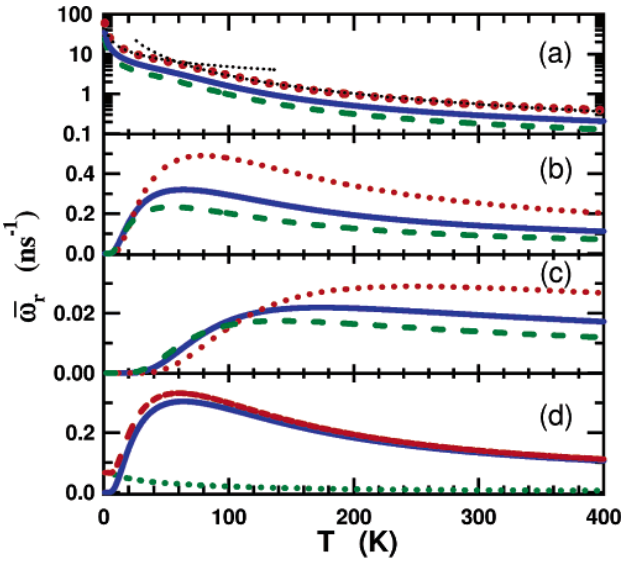

Figure 4 Calculated temperature dependent radiative decay rate for (a–c) three zigzag nanotubes with 1.0 nm (dotted red), 1.5 nm (solid blue), and 2.0 nm (dashed green) diameters under different thermalization conditions. a) The case of thermalization only within the optically active bands. b) Effect of thermalization within the entire singlet manifold. c) Thermalization between all spin and parity states. d) is the radiative decay rate including redistribution of oscillator strength due to disorder induced symmetry breaking for a 1.0 nm diameter tube with the contribution of the low lying, even symmetry state (dotted green), the higher energy, odd symmetry state (solid blue), and the total (dashed red). (Reproduced from Perebeinos et al. [52])

performed *ab initio* calculations of radiative decay rates in SWNTs. Within the approximation that the allowed energy range is much less than the thermal energy ($\Gamma \ll k_{\mathrm{B}}T$) they come to the same conclusion when including only the bright band, a $1/\sqrt{T}$ scaling behavior.

As nanotubes have a complex exciton manifold (Fig. 2), we must consider contributions from various states to radiative decay. The existence of a low-lying optically inactive band complicates this process. Spataru et al. [53] and Perebeinos et al. [52] calculated the temperature dependent radiative decay rate for SWNTs. Fig. 4a–c show the effect of various mixing between bright and dark states for three different diameter tubes (1 nm - dotted red, 1.5 nm - solid blue, and 2 nm - dashed green), calculated by Perebeinos et al. [52]. Fig. 4a shows radiative decay rate as a function of temperature for the case of thermalization only within the bright bands. As the temperature is decreased, so too is the number of thermally populated states with momentum $> \kappa$, increasing the relative population in the optically allowed momentum states and, therefore, the overall photoluminescence intensity.

Fig. 4b demonstrates the case of complete thermalization between different parity states within the singlet manifold. In this case, excitons are allowed to scatter into the even parity, optically forbidden band. This captures a large portion of the exciton population at low temperature, resulting in a downturn of radiative decay rate and photoluminescence intensity. Fig. 4c includes singlet and triplet states of even and odd parity, the full 16 states of the first exciton manifold. In this case, the peak in radiative decay rate is shifted to a higher relative temperature. This is due to the large induced exchange splitting between the singlet and triplet states (a factor of five larger than the even-odd parity splittings in this calculation) that results in a trapping of the exciton population in optically inactive states at a higher temperature.

2.4. SWNTs in a magnetic field

Arising from the interplay of the Aharonov-Bohm effect and the Bloch theorem, the band structure of a SWNT can be modified by an applied magnetic field [66–69]. When a nanotube is threaded by an amount of magnetic flux, ϕ, an Aharonov-Bohm phase modifies the circumferential boundary conditions on the electronic wavefunctions, breaking time reversal symmetry and lifting valley degeneracy. The resulting band structure is predicted to oscillate with a period of the flux quantum, $\phi_0 = e/h$, where e is the electron charge and h is Planck's constant. The field required for a full oscillation ($\phi = \phi_0$) in a 1 nm diameter nanotube is on the order of thousands of tesla. In the region of readily accessible fields ($\leq$60 T) the band gap of a semiconducting (metallic) SWNT will shrink (open)

with applied field as the K and K′ valleys split in energy, resulting in peak splittings and shifts in optical spectra.

Breaking time reversal symmetry also lowers the amount of short-range Coulomb mixing between the valleys. Within the singlet states, this mixes the even and odd parity excitons of zero angular momentum, resulting in spectral weight and effective mass redistribution. At very high fields this results in the recovery of the direct K and K′ excitons with similar spectral weights and effective masses. Thus, the Aharonov-Bohm effect is expected to have three main observable conditions in optical spectroscopy of semiconducting SWNTs in a parallel magnetic field: peak position shift [66], spectral weight redistribution [70], and effective mass redistribution [39].

Fig. 5 shows interband optical absorption spectra, calculated by Ando [70], using a $\mathbf{k}\cdot\mathbf{p}$ model in the presence of Coulomb mixing at various values of nanotube threading flux. At zero field, there is a single absorption peak originating from the optically active, odd parity, singlet

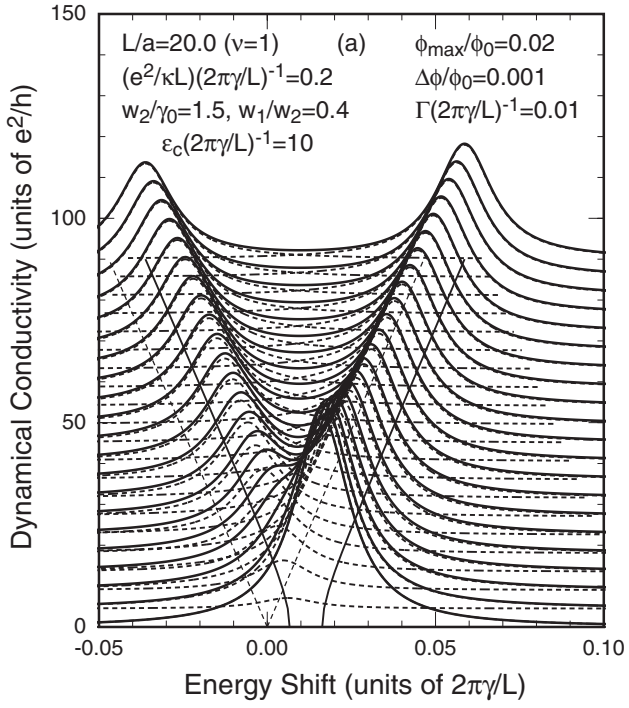

Figure 5 Magnetic field dependent dynamical conductivity for a semiconducting nanotube, analogous to absorption spectra, at flux intervals of .001 from 0 to 0.02 ϕ_0. When there is no threading flux, only the peak originating from the bright singlet exciton is visible. As the amount of threading flux is increased, spectral weight redistributes between the two peaks in such a way that the (originally) dark exciton state increases in intensity at the expense of the (originally) bright exciton as their positions shift apart. The peak positions of the two zero angular momentum singlet excitons are represented by the solid lines in the presence of exchange mixing and by dashed lines with no mixing. Traces are vertically offset for clarity. (Reproduced from Ando [70])

state. As the magnetic field is increased, and the states are mixed, the absorption peak splits into two, and the spectral weight is redistributed between them. The originally dark exciton's oscillator strength is increased through magnetic brightening. For these effects to be observable, the strength of the exciton mixing must be comparable to the zero field exchange energy splitting, $\Delta_{\rm x}$. The magnetic-field-induced mixing is proportional to the nanotube threading magnetic flux ($\phi = \pi B d^2/4$) such that the Aharonov-Bohm mixing is $\Delta_{\rm AB} = \mu\phi$, where B is the magnetic field strength, d is the nanotube diameter, and μ is a proportionality constant. It is also important to note that μ is dependent on the alignment of the nanotubes with respect to the magnetic field [37]. Certain nanotube impurities are also expected to break time reversal symmetry, resulting in wavefunction mixing and finite brightening of the dark exciton at zero magnetic field. Thus, a finite amount of disorder-induced mixing, $\Delta_{\rm dis}$, can be added to $\Delta_{\rm AB}$ [39].

Using a simplified two-level model, the exciton dispersions in the presence of mixing ($\Delta_{\rm AB} \neq 0$) are given by [39]

$$\epsilon_{\delta,\beta}(K) = \frac{1}{2}\left[E_\delta(K) + E_\beta(K) \mp \sqrt{[E_\delta(K) - E_\beta(K)]^2 + {\Delta_{\rm AB}}^2}\right], \quad (1)$$

where $E_\beta(K)$ and $E_\beta(K)$ are the zero field dispersions of the lowest energy dark and bright bands (Fig. 3). The relative oscillator strengths of the dark and bright excitons are given by

$$I_{\delta,\beta} = \frac{1}{2} \mp \frac{1}{2}\frac{\Delta_{\rm x}}{\sqrt{{\Delta_{\rm x}}^2 + {\Delta_{\rm AB}}^2}} \quad (2)$$

where $\Delta_{\rm x} = \Delta_\beta - \Delta_\delta$ is the dark-bright energy splitting in zero magnetic field. In the absence of a magnetic field, the effective mass of the bright exciton is predicted to be much less than that of the dark exciton [52]. The magnetic field dependence of the effective mass $m_i^*(B)$ is

$$\frac{1}{m_\delta^*(B)} = \frac{I_\beta}{m_\delta^*} + \frac{I_\delta}{m_\beta^*}, \quad \frac{1}{m_\beta^*(B)} = \frac{I_\beta}{m_\beta^*} + \frac{I_\delta}{m_\delta^*}. \quad (3)$$

Fig. 6a plots the magnetic field, and hence $\Delta_{\rm AB}$, dependence of the relative oscillator strengths of the dark and bright bands for a (9,4) nanotube in a parallel magnetic field with zero non-magnetic-field-induced symmetry breaking ($\Delta_{\rm dis} = 0$). At zero field, the bright state has 100% of the total spectral weight. As the time reversal symmetry of the system is broken by finite amounts of $\Delta_{\rm AB}$, the oscillator strength redistributes between the bright and dark states. At high values of magnetic field, the states approach similar spectral weights and effective masses. Fig. 7 shows the dispersions of the bright and dark states at zero field and at high field for the same (9,4) nanotube. The evolution of the peak positions with field is plotted in Fig. 6b.

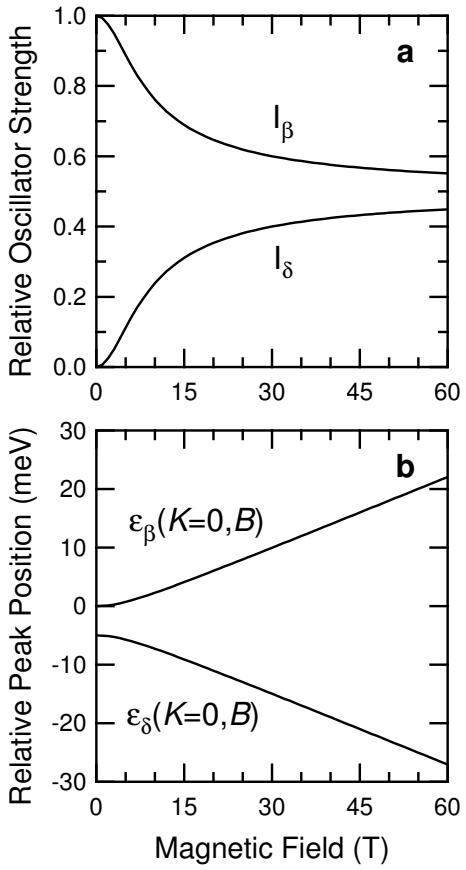

Figure 6 Relative oscillator strength (a) and relative peak position shift (b) for the low lying bright (β) and dark (δ) bands of the (9,4) nanotube. Relative oscillator strength equalizes at high fields due to Δ_{AB} induced wavefunction mixing. Peak postion shifts were determined from the K=0 values of the dispersions calculated in Eq. (1).

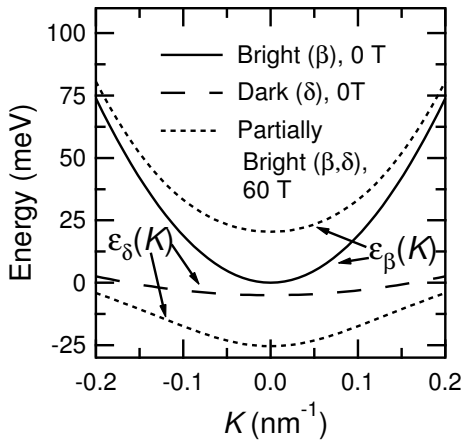

Figure 7 Calculated dispersions for the lowest energy bright and dark exciton bands of a (9,4) nanotube at 0 T and 60 T from Eq. (1).

2.5. Symmetry breaking effect on radiative decay in SWNTs

The effect of symmetry breaking on the temperature dependence of the radiative decay rate can now be considered. In order for phonons to effectively scatter excitons between bands, there must be finite symmetry breaking. Fig. 4d plots a partial mixing (5%) of even and odd parity states within the singlet bands for a 1.5 nm diameter tube [52]. The individual traces show the contributions from the lower energy dark state of even parity (dotted green), from the bright state of odd parity (solid blue), and the combination of the two (dashed red). Even this amount of mixing greatly modifies the ideal picture of Fig. 4b. This behavior should manifest in measured spectra as a satellite peak with lower emission energy of negligible intensity at high temperature, but becoming dominant at lower temperature.

Application of a magnetic field redistributes the spectral weight according to Eq. (2). At low temperature, when excitons are trapped in the optically inactive state, this will result in a dramatic increase in photoluminescence intensity. This process of magnetic brightening was recently independently observed by two groups [38, 39]. Starting from our calculated dispersions of the the two lowest lying bands, we can get the temperature and magnetic field dependence of the measured photoluminescence intensity.

$$\gamma \propto \frac{1}{\sqrt{T}} \frac{\frac{I_\delta(B)}{I_\beta(B)} + e^{\frac{-\sqrt{{\Delta_x}^2+{\Delta_{AB}}^2}}{k_B T}}}{\sqrt{\frac{m^*_\delta(B)}{m^*_\beta(B)}} + e^{\frac{-\sqrt{{\Delta_x}^2+{\Delta_{AB}}^2}}{k_B T}}} \tag{4}$$

Eq. (4) reproduces the peak behavior as a function of T predicted by Perebeinos et al. at finite temperature in the absence of symmetry breaking, at zero magnetic field [52]. Once the field is applied, the peak behavior disappears, eventually recovering the single band temperature dependence, $\propto 1/\sqrt{T}$, at very high fields.

These calculations show that the optical properties of SWNTs are highly sensitive to symmetry affecting phenomena. In particular, any effects that break time reversal symmetry in nanotubes result in both thermalization between typically forbidden bands and redistribution of the oscillator strength. As we have shown, a controllable way to break symmetry is by the Aharonov-Bohm effect via an applied parallel magnetic field. The direct control of both temperature and magnetic field should reveal the nature of the excitonic structure in SWNTs.

3. Experiment

3.1. Samples for optical study

Choice of sample is important in any optical experiment on carbon nanotubes because they are 100% surface and

easily influenced by environmental factors. Nanotubes can be produced in small amounts on surfaces via chemical vapor deposition with localized catalysts for use in individual nanotube experiments, or in bulk quantities in gas phase reactors such as the High Pressure CO (HiPco) process [71] or on a zeolite-supported catalyst like CoMoCAT [72]. These fabrication techniques involve decomposition of a carbon rich feedstock gas (carbon monoxide, methane, ethanol, etc.) on the surface of nano-sized catalyst particles such as Fe, Mo, and Co.

While both bulk materials and individually grown nanotubes have the potential to be used in optical experiments, there are many factors that must be considered. When produced on surfaces, unless special steps such as growing over trenches, between pillars [73], or use of non-pertubative substrates are taken, surface interactions strongly quench observable photoluminescence. In bulk samples, nanotubes are produced in large bundles, or ropes, where they are in van der Waals contact, and must be liberated from them in order to observe photoluminescence. Samples often contain high amounts of residual catalyst particles as well. Purification procedures often involve harsh acids which can damage nanotubes and quench optical properties.

To date, the most efficient way to separate nanotubes from their large ropes is a sonication in surfactant solution followed by ultra-centrifugation [15]. In this procedure, nanotubes are initially dispersed in any one of a number of surfactant solutions [74], mixed at high sheer, sonicated at high power, and ultra-centrifuged. High sheer mixing breaks up macroscopic aggregates, and sonication exfoliates roped nanotubes, resulting in a mixture of bundles and individualized nanotubes covered in surfactant. In the centrifugation step, as the density of a bundle of nanotubes covered in surfactant is higher than that of an individual nanotube, the bundles aggregate into a pellet at the bottom of the centrifuge tube. The resulting supernatant can be readily decanted and shows sharp absorption features and strong photoluminescence.

As SWNTs' band structure depends not only on their diameter but also their chiral angle, a bulk sample containing many species of SWNTs shows a number of spectral features. In a typical HiPco batch, there are >30 different species of nanotubes present [19]. Though this heterogeneity helped in the initial assignment of spectral features to specific chiralities of nanotube [18], it complicates spectroscopic measurements where it is desirable to focus on one species of tube. Different methods of production can narrow the distribution of produced chiralities. Under certain reactor conditions, CoMoCAT produces mainly four types of semiconducting nanotubes [75], but there is not yet any method to produce a single species in bulk quantities. Recent studies have utilized density gradients to achieve limited quantities of single species samples [40, 41]. This mechanism also removes a larger fraction of residual non-nanotube material and bundles, allowing for more detailed studies of species specific properties [48, 49].

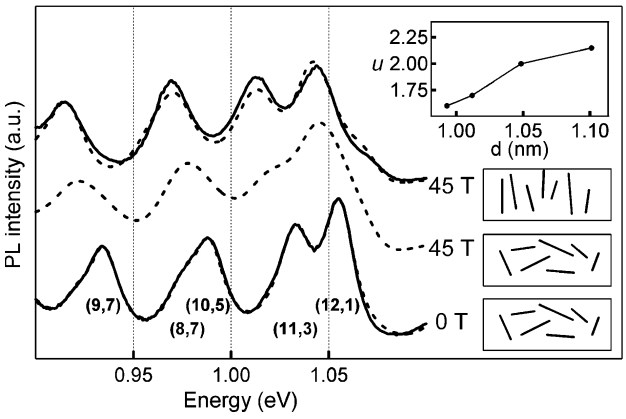

Figure 8 Magneto-photoluminescence spectra of an aqueous suspension of SWNTs taken at 0 T and 45 T and room temperature (solid lines). A large spectral red shift (∼1 meV/T) is observed. Accompanying simulated spectra (dashed lines) are shown at 0 T and 45 T with red shifts and both with and without alignment at 45 T. Diameter dependent, dimensionless alignment energies u (Eq. (6)) used to simulate the four main peaks in the 45 T spectra are shown in the inset. (Reproduced from Zaric et al. [36])

3.2. *Magnetic field dependence*

When a nanotube is threaded by an amount of magnetic flux, its bandgap is modified by an Aharonov-Bohm phase, as described by Ajiki and Ando [66] and observed by Zaric et al. [35]. Fig. 8 shows magneto-photoluminescence spectra using the 45 T hybrid magnet at the National High Magnetic Field Laboratory in Tallahassee, FL, collected from an aqueous surfactant suspension of HiPco SWNTs at room temperature. Photoluminescence was excited with a CW Ti:Sapphire laser tuned to 795 nm (1.56 eV) to be resonant with the main peaks (with indicated chiralities) in the spectra. At high field all the peaks are red-shifted, demonstrating the predicted bandgap shrinkage due to an Aharonov-Bohm phase.

The relatively small bore of high field magnets (as low as 7 mm in some pulsed magnets) require carefully designed sample holders with optical fibers. Often, use of polarizers and collimating optics is difficult or impossible, complicating the traditional measurement geometries. The Faraday geometry (light propagation vector parallel to the magnetic field and polarization vector perpendicular to it) and the Voigt geometry (light propagation vector perpendicular to the magnetic field and polarization vector parallel or perpendicular to it) can only be defined when the light is collimated and properly polarized. As nanotubes strongly absorb light polarized along their long axis [67], and the Aharonov-Bohm phase only modifies the band structure of a SWNT that is threaded with flux, use of a pseudo-Voigt geometry is necessary for observation of magnetic brightening. In this case, the nanotube alignment is placed parallel to the magnetic field and with the laser

light (turned by a prism or mirror) incident perpendicular to the magnetic field.

In water-surfactant suspensions, nanotubes are free to undergo Brownian motion, or thermally activated random motion. Carbon nanotubes have anisotropic magnetic susceptibilities [76, 77]. Metallic tubes are paramagnetic parallel and diamagnetic perpendicular to their long axis, while semiconducting tubes are diamagnetic on both axes with the perpendicular magnitude being larger, hence both types of nanotubes will align in a magnetic field. The competition between these two energies defines the overall amount of alignment for one tube [Eq. (6)]. These alignment effects have been observed in various experiments [78–81]. This complicates analysis of magnetic field dependent spectra as the nanotubes have a varying amount of alignment energy at different fields, which leads to a varying amount of threading flux.

An alignment distribution function [79] ($P(\theta)$) based on the applied magnetic field (B), the angle of the tube with respect to the magnetic field (θ), the moles of carbon atoms in the tube (N), and the magnetic susceptibility anisotropy ($\Delta\chi$) [36] can be calculated as

$$\frac{dP(\theta)}{d\theta} = \frac{e^{-u^2 \sin^2\theta} \sin\theta}{\int_0^{\pi/2} e^{-u^2 \sin^2\theta} \sin\theta d\theta}, \qquad (5)$$

where u is the dimensionless alignment energy:

$$u = \sqrt{\frac{B^2 N \Delta\chi}{k_B T}}. \qquad (6)$$

To show the importance of fitting the data with the correct alignment energy and hence angular distribution, Eq. (5) and Eq. (6) are used to reproduce the spectra at 45 T in Fig. 8. Both dashed lines are modeled with the same amount of Aharonov-Bohm-effect-induced splitting. The isotropic distribution, not accounting for alignment factors, does not correctly reproduce the experimental result.

This data is optical proof of the influence of the Aharonov-Bohm phase on the band structure of SWNTs. As photoluminescence experiments are influenced by excitonic population as well as oscillator strength, the observed band gap shift in Fig. 8 is dominated by the lower energy peak. Absorption spectroscopy, on the other hand, can directly observe the change in oscillator strength and peak position shift as a function of magnetic field, as demonstrated by a recent study using magnetic fields up to 75 T [37]. However, absorption measurements include contributions from all species present in the sample, leading to significant inhomogeneous broadening. Careful choice of excitation wavelength or use of full photoluminescence excitation spectroscopy has the advantage of allowing for selection of a limited number of species. To further the study of the excitonic structure of SWNTs through photoluminescence, we must also control the exciton state population through temperature dependent studies.

3.3. Temperature dependence

At low temperature, various techniques can be used to compensate for local environmental changes. This is a sensitive issue as nanotubes are 100% surface atoms and can be influenced by variations in their surroundings. In this section, we will discuss results from frozen suspensions, gelatin films, pillar suspended individual nanotubes, and individual nanotubes spun coat from suspensions on to glass substrates. The factors influencing nanotubes in each of these environments must be taken into consideration when interpreting results.

When bulk suspensions are used, micelle integrity and strain induced by freezing water can be an issue. Flash freezing [38], addition of materials to suppress the freezing point of water [82], or use of a solid matrix such as gelatin [39, 83–85] are viable techniques for accessing low temperature ranges. While freezing the solution quickly circumvents the destabilization of the micelle at intermediate temperatures, it also induces ice phase dependent strain on the nanotubes that result in bandgap shifting [86]. Ice also affects the opacity of the solution, hindering signal collection. Additives such as glycol will suppress the freezing point of water, extending the available range of measurement down to ~200 K, avoiding possible strain-induced complications, but only down to ~200 K. Use of solidified samples that preserve the local environment of the nanotube are therefore a more ideal approach. Gelatin with a low melting point (~40° C) can be added to a gently heated nanotube solution before casting it on a surface. This technique has the benefit of minimally disturbing the micelle, while maintaining sharp absorption features and strong luminescence intensity.

The inset of Fig. 9 shows a typical photoluminescence excitation map at low temperature with a CW Ti:Sapphire laser as an excitation source taken by Mortimer et al. [38]. The eight traces in Fig. 9 show the temperature dependence of different species extracted from several maps. As the temperature is decreased to ~40 K, the overall intensity of photoluminescence increases. Matching with theory we have reviewed, this is due to concentration of excitons in $K < \kappa$ states. When the temperature is further decreased from 40 K to 4 K, however, the overall intensity *decreases*. This deviation from the expected $1/\sqrt{T}$ dependence for simple 1D systems is indicative of a low energy trap state influencing the radiative decay process. Each nanotube species has a different peak temperature. This is expected as the splitting between the lowest energy, optically inactive state and the higher energy, bright state is predicted to depend on the nanotube chirality [52, 53].

Utilizing a gelatin stabilized sample, Berger et al. measured time-resolved photoluminescence from predominately (9,4) nanotubes [83]. Ti:Sapphire laser pulses of 1.4 ps tuned to 730 nm (1.7 eV) were chosen as an excitation source to be resonant with the (9,4) nanotube. The photoluminescence signal was dispersed on a monochromator for detection with an infrared sensitive streak camera. They collected spectrally integrated (from 1.08 to

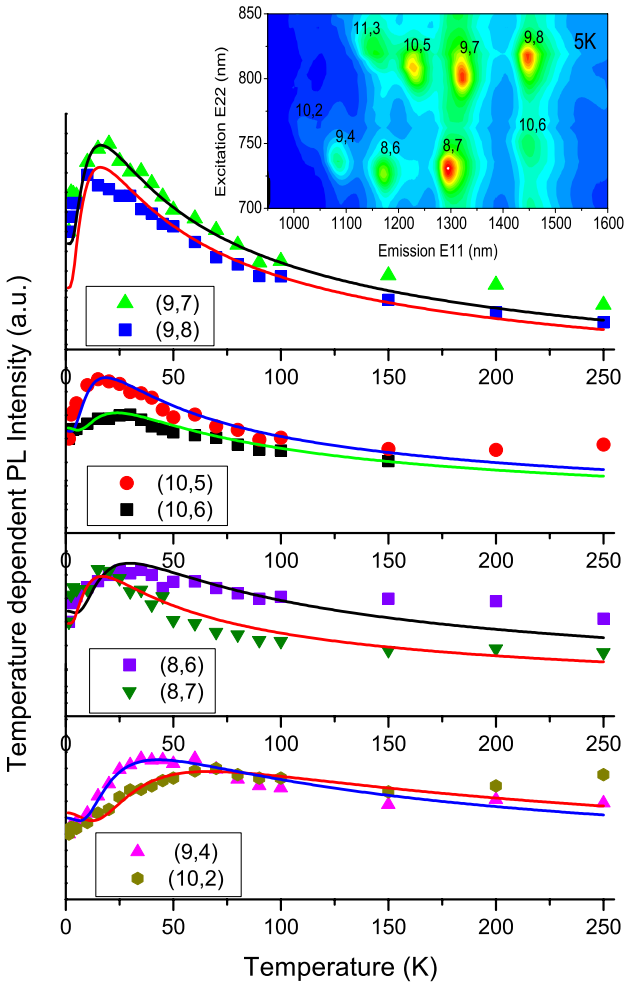

Figure 9 Measured temperature dependence of photoluminescence intensity of eight semiconducting SWNT chiralities (solid markers). To ensure on resonance measurement, intensities were extracted from photoluminescence excitation maps in the Ti:Sapphire excitation range (typical map at 5 K shown in inset). As the temperature is decreased, the photoluminescence intensity increases and peaks in the range of 20 K to 50 K before falling off sharply. Fits to the data are represented by solid lines. (Reprinted with permission from I. B. Mortimer and R. J. Nicholas [38]. Copyright 2007 by the American Physical Society.)

1.165 eV) time-resolved photoluminescence from room temperature to 10 K, displayed in Fig. 10a. The minimum time resolution of the setup was ∼25 ps. The excitation fluence was maintained both in the linear regime and low enough to preclude any effects resulting from heating the nanotubes. Two decays are observed: the initial fast decay is temperature-independent and likely non-radiative in origin, while the longer decay at times >100 ps is due to a combination of radiative and non-radiative lifetime. There is a dramatic change in the measured signal as a function of temperature. At high temperatures, the photoluminescence decays quickly due to the presence of non-radiative channels as shown by the overall low intensity of photoluminescence at high temperatures. As the temperature is decreased, the long decay component increases. Fig. 10b shows both CW and temporally integrated temperature-dependent normalized photoluminescence intensity. There is a peak at finite temperature, ∼40 K, similar to Mortimer and Nicholas [38].

In order to mitigate environmental interactions, Lefebvre and coworkers chose to use nanotubes suspended from pillars for their temperature-dependent photoluminescence studies [32]. Samples were grown using methane chemical vapor deposition on patterned Si/SiO_2 substrates [73]. These samples are individuals that show strong photoluminescence, yet are free from surfactant and exposed to atmosphere. In Fig. 11 the temperature-dependent photoluminescence of five nanotube species extracted from ensemble measurements on a pillar-suspended sample is shown. The photoluminescence intensity shows an increase when the temperature is decreased to ∼40 K followed by a decrease when the temperature is lowered to 4 K, matching with predictions and other observations. Adding a microscope objective to their setup and zooming in on a single tube, spectra such as Fig. 12a can be collected. As the temperature is reduced, from 18 K to 5 K, multiple peaks suddenly appear below 10 K. These extra peaks could be due to various exciton localization effects such as trapping at ends or defects, phonon replicas, or excitonic levels. In order to investigate the nature of these peaks, one needs an independent control of the valley degeneracy. If any of these peaks respond to a symmetry breaking magnetic field, it is an indication that they are related to dark excitonic levels.

Another example of multiple peaks in single SWNTs can be seen in Fig. 12b [28]. Collected from a (6,4) nanotube spun from solution onto glass, these temperature dependent spectra show two peaks at all temperatures measured, with a transfer of population to the lower energy peak as the temperature decreases. This data is consistent with predictions made by Perebeinos et al. [52] about lower energy states being related to excitonic levels. However, in order to completely determine this, additional measurements are required, specifically the application of a magnetic field.

3.4. Temperature and magnetic field dependence – magnetic brightening

The combination of temperature and magnetic-field-dependent measurements allows for control of population and oscillator strengths. This hybrid technique enables unambiguous identification of predicted dark and bright excitonic levels. The phenomenon of magnetic brightening, restricting excitons to the lower lying, dark exciton band and then activating that level with a magnetic field, conclusively proves the existence of dark excitons and demonstrates their influence on the photoluminescence

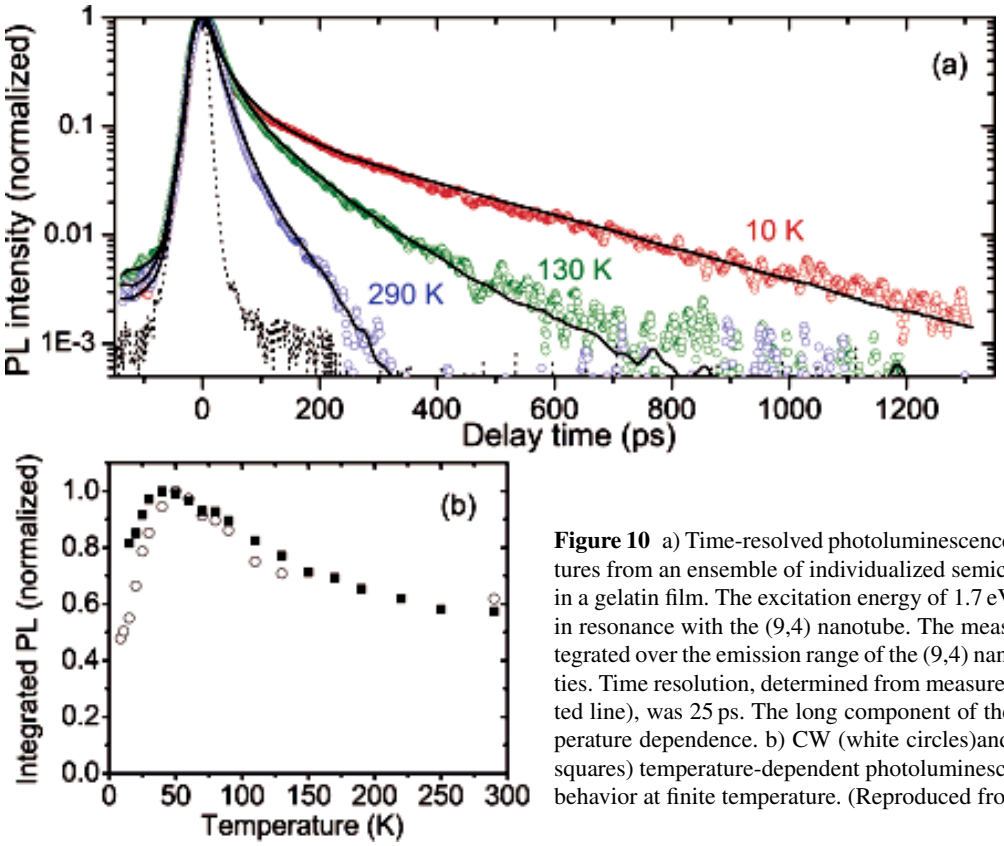

Figure 10 a) Time-resolved photoluminescence at various indicated temperatures from an ensemble of individualized semiconducting SWNTs suspended in a gelatin film. The excitation energy of 1.7 eV (729.5 nm) was chosen to be in resonance with the (9,4) nanotube. The measured signal was spectrally integrated over the emission range of the (9,4) nanotube to exclude other chiralities. Time resolution, determined from measurement of system response (dotted line), was 25 ps. The long component of the decay exhibits a strong temperature dependence. b) CW (white circles)and temporally integrated (black squares) temperature-dependent photoluminescence intensity showing a peak behavior at finite temperature. (Reproduced from Berger et al. [83].)

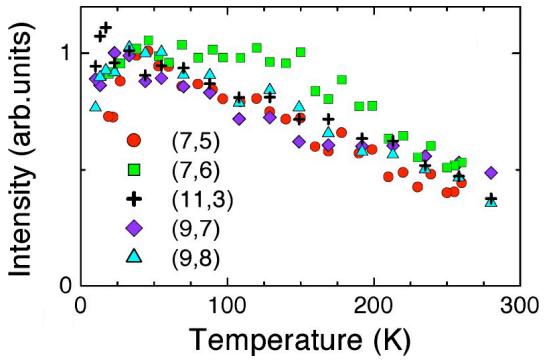

Figure 11 Integrated normalized photoluminescence intensity of 5 chiralities of semiconducting SWNTs, extracted from ensemble measurements, as a function of temperature. Showing peak behavior in temperature. (Reprinted with permission from J. Lefebvre, J. M. Fraser, P. Finnie, and Y. Homma [33]. Copyright 2004 by the American Physical Society.)

properties of semiconducting SWNTs. Two studies of this phenomenon have recently been performed, up to 19.5 T [38] and up to 56 T [39] in DC and pulsed magnetic fields, respectively.

The two studies utilized solid samples discussed in Sect. 3.1. Mortimer and Nicholas [38] used frozen decanted solutions with isotropic alignment distributions while Shaver et al. [39] used stretch-aligned gelatin films. Solidified samples are imperative when measuring magnetic-field-dependent photoluminescence intensity as they eliminate the need for de-convolution of dynamic magnetic alignment [87]. When a gelatin film is used, it is possible to stretch it, aligning the nanotubes as the film is pulled. The overall alignment is characterized by the nematic order parameter, which can be measured through polarized absorption [88]. Aligned samples sharpen the distribution function [Eq. (5)], maximizing the total flux threading all the nanotubes. Other polymers such as polyacrlyic acid have recently been used to disperse and align nanotubes to a very high degree [89]; these also permit the accurate measurement of perpendicular-field effects [90].

Shaver et al. [39] performed measurements up to 56 T at the Laboratoire National des Champs Magnétiques Pulsés in Toulouse, France. The magnetic field was generated from a 3 MJ, 100 ms capacitively-driven current pulse with a 25 ms rise time and exponential fall-off (plotted in Fig. 13a). While the nature of a pulsed field puts rather stringent requirements on the acquisition time of a photoluminescence experiment ($\sim$1 ms) in order to keep reasonable magnetic field resolution and the efficiency of collection within the sample probe, the time-dependent spectra taken during one magnetic field pulse strikingly show the effect of magnetic brightening. Fig. 13b shows typical data collected during one magnetic field pulse. At low temperature the magnetic field dramatically increases the

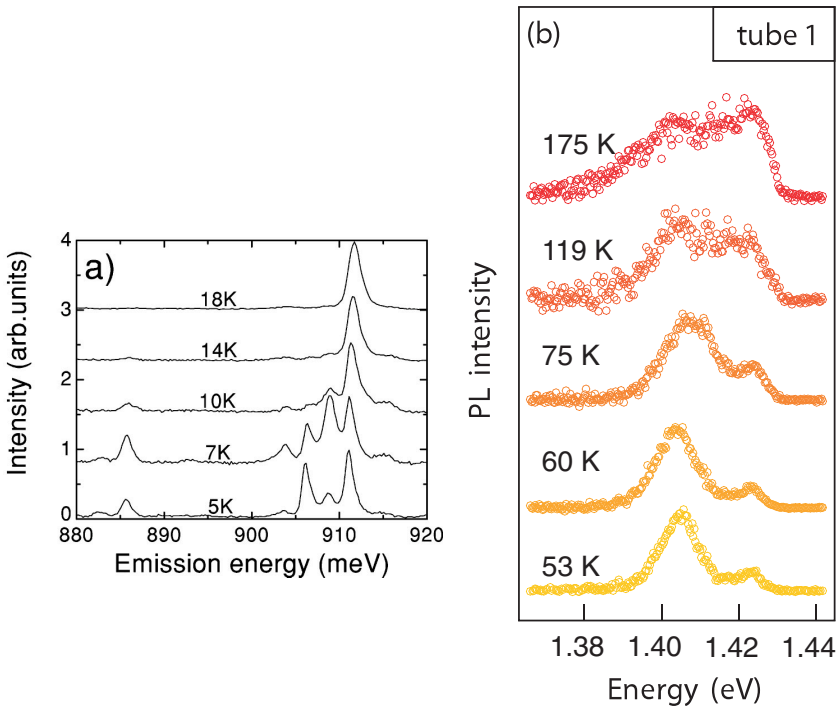

Figure 12 a) Photoluminescence (λ_{ex}= 796 nm, 1.557 eV) from an individual (9,8) nanotube at low temperature. Below 14 K multiple peaks appear in the spectra. (Reproduced from Lefebrev et al. [33]) b) Photoluminescence spectra for an individual (6,4) tube from 53 K to 175 K (λ_{ex} = 800 nm, 1.55 eV). Two peaks are clearly visible from an individual semiconducting SWNT. As the temperature is reduced the higher energy peak loses intensity. (Reprinted with permission from A. Hagen et al. [28]. Copyright 2005 by the American Physical Society.)

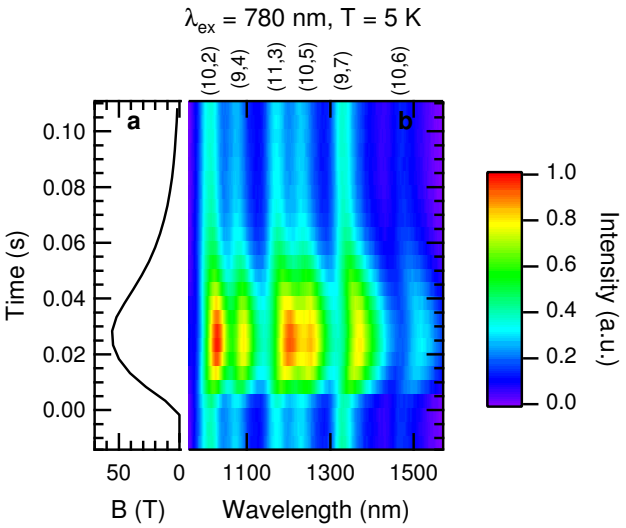

Figure 13 Magnetic brightening of SWNT photoluminescence. The applied time-dependent magnetic field is shown in part a. Part b shows the measured photoluminescence spectra every ∼5 ms. As the magnetic field is applied, a ∼4 fold increase in photoluminescence intensity and a significant red shifting of peaks is observed. (Reproduced from Shaver et al. [39])

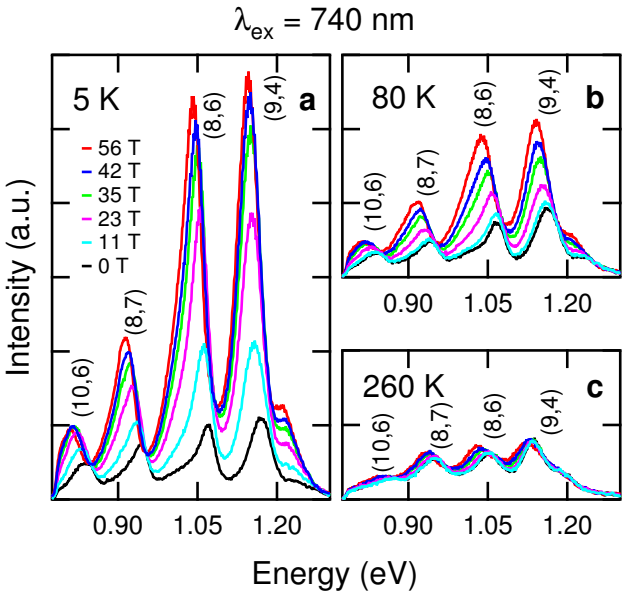

Figure 14 Magneto-photoluminescence spectra of a static nanotube/gelatin film at a) 5 K, b) 80 K, and c) 260 K with an excitation wavelength of 740 nm. Nanotube chirality and magnetic field are indicated. As the magnetic field is applied, there is a red shift of peaks at all temperatures. Also, there is a dramatic increase in photoluminescence intensity with applied field at low temperature, a modest increase at intermediate temperature, and a negligible increase at high temperature. The high temperature data shows a slight change in lineshape on the high energy side of the peaks due to the finite occupation of the higher energy exciton peak. (Reproduced from Shaver et al. [39])

photoluminescence intensity and red-shifts the peak positions through the Aharonov-Bohm effect.

Fig. 14 displays spectral slices taken at several time points in three different experiments. Fig. 14a shows the most dramatic effect at 5 K. The magnetic field red-shifts the peak positions and dramatically increases the overall photoluminescence intensity by a factor of ∼5. At the in-

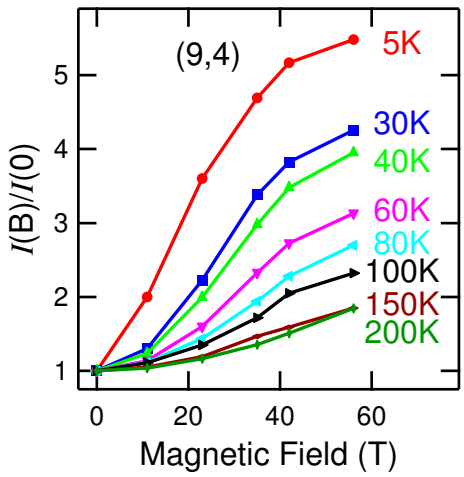

Figure 15 Integrated photoluminescence intensity of a (9,4) nanotube, normalized to the zero-field value, as a function of magnetic field at indicated temperatures. Clearly displays amount of magnetic brightening increasing for decreasing temperature. (Reproduced from Shaver et al. [39])

termediate temperature of 80 K (Fig. 14b), the peaks redshift by the same amount, but the intensity increase is only ∼2 due to the broader thermal distribution of excitons. 260 K spectra from Fig. 14c show negligible intensity increase, but still display a red shift. The peaks also broaden, indicating the partial thermal population of the higher energy, formerly bright state.

Spectra displayed in Fig. 14 can be analyzed to obtain the integrated peak intensity for each chirality present in the sample. Normalized integrated intensity for the (9,4) nanotube vs. magnetic field is shown in Fig. 15 between 5 K and 200 K. This figure summarizes the relative increase, magnetic brightening, vs. magnetic field. At high temperatures, the increase is ∼2, while at low temperatures it is ∼5. The non-normalized data is shown vs. temperature in Fig. 16a. The zero-field photoluminescence shows an increase in intensity as the temperature is decreased to 40 K, as dark states that do not satisfy energy-momentum conservation are depopulated. Below 40 K the intensity decreases due to population trapping in the dark state. When the magnetic field is turned on and the lower state gains oscillator strength, the peak behavior in intensity is lost as the dark trap state is brightened. A simple simulation, based on the two-level model of Eq. (4), is shown in Fig. 16b. The salient features of the intensity dependence are reproduced, including the peak behavior at zero field and the increase in intensity at finite field.

Mortimer and Nicholas [38] used DC fields up to 19.5 T to perform temperature-dependent magneto-photoluminescence measurements. Their samples were frozen aqueous suspensions with strain-induced bandgap shifts [86]. To ensure on-resonance excitation over a large temperature and magnetic field range, they measured photoluminescence excitation maps. Fig. 17 shows

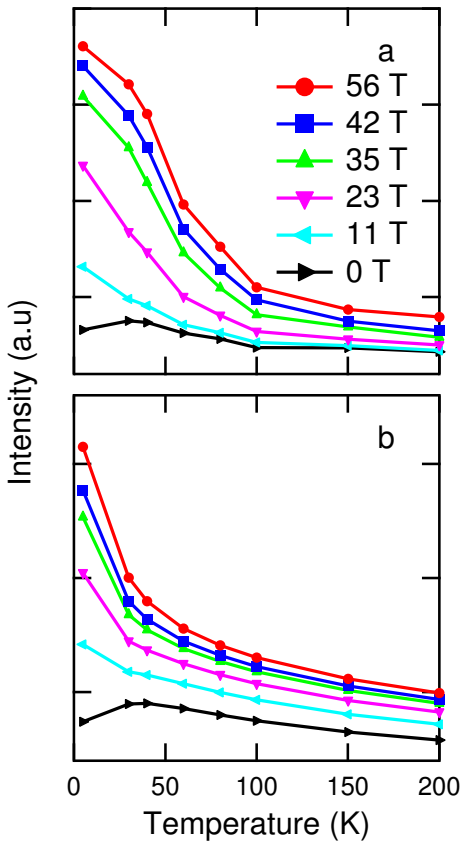

Figure 16 a) Integrated photoluminescence intensity of a (9,4) nanotube extracted from ensemble measurements (excitation wavelength of 740 nm) as a function of temperature at indicated fields. b) Simulated integrated photoluminescence intensity using Eq. (4)

temperature-dependent intensity of the (9,4) and (10,5) nanotubes at 0 T and 19.5 T. This data also matches well with the proposed model. The solid lines are best fit lines deducing the amount of Δ_x for each tube, utilizing a similar two-level model to that described here.

4. Conclusion and outlook

We have reviewed recent measurements of magnetic field and temperature-dependent photoluminescence spectroscopy of semiconducting SWNTs. While temperature dependence of photoluminescence can show the influence of dark states on radiative decay in these 1D systems, the application of a magnetic field is necessary to elucidate the nature of those states. Thus, the combination of temperature for population control and magnetic field for symmetry control is a powerful technique for examining the nature of excitonic transitions in SWNTs.

Though progress has been made in clarifying the influence of intrinsic dark states on the radiative decay process, there are many questions left unanswered. Among

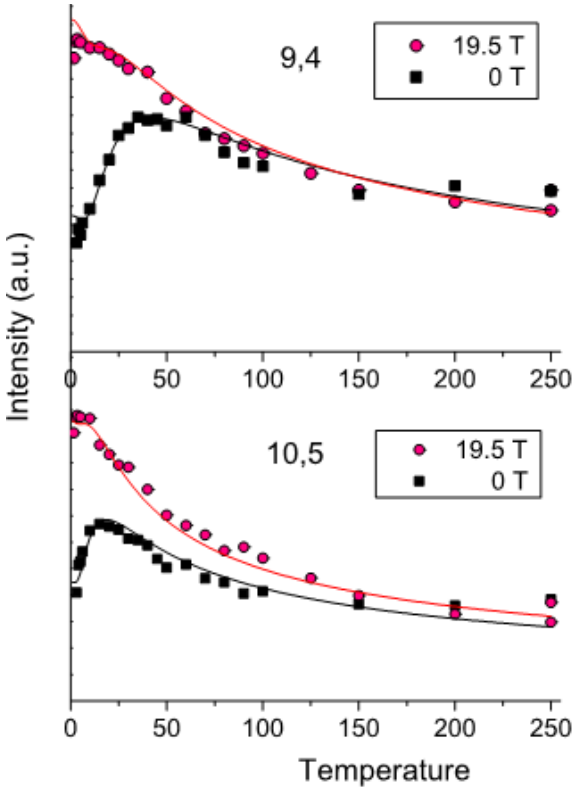

Figure 17 Temperature-dependent photoluminescence intensity measured at 0 T and 19.5 T for (9,4) and (10,5) nanotubes (extracted from excitation maps). The solid lines are fit using a two level model with magnetic-field-dependent oscillator strengths. The emission intensity increases greatly at low temperatures with the application of magnetic field. (Reprinted with permission from I. B. Mortimer and R. J. Nicholas [38]. Copyright 2007 by the American Physical Society.)

these are the influence that self trapping, defects, and other forms of localization have on the radiative decay. Recent microscopy on individual tubes has shown that a single defect will quench photoluminescence over ∼100 nm, opening the possibility to study nanotubes with a controlled amount of defects [91]. The temperature at which exciton scattering processes become inefficient, resulting in non-thermal distributions, is yet to be determined. To what extent non-radiative effects depend on temperature and magnetic field is also an open question. Further temperature and magnetic-field-dependent studies are thus required. In particular, single SWNT microscopy at low temperature with an applied magnetic field and varying amounts of induced defects could help to uncover the physics of some of these effects. Knowledge gained through the direct control of the photoluminescence of individual SWNTs could lead to applications in devices.

Acknowledgements This work was performed with the support of the Robert A. Welch Foundation (through Grant No. C-1509), the National Science Foundation (through Grants Nos. DMR-0134058, DMR-0325474, OISE-0437342, and OISE-0530220), and EuroMagNET under the EU Contract No. RII3-CT-2004-506239 of the sixth Framework "Structuring the European Research Area, Research Infrastructures Action". We also thank our collaborators Vasili Perebeinos, Oliver Portugall, Vojislav Krstić, Geert Rikken, Yuhei Miyauchi, and Shigeo Maruyama. The authors also thank David Hilton and Ajit Srivastava for helpful discussions.

Jonah Shaver, born in 1982, received his B.S. degree in physics from Wright State University (Dayton, Ohio) in 2002. Accepted into the Ph.D. program in applied physics at Rice University (Houston, Texas) he worked under the advisement of Richard E. Smalley on time-dependent Raman and photoluminescence of single-walled carbon nanotube oxidation kinetics until 2005. He joined the research group of Prof. Junichiro Kono in January 2005 and specializes in carbon nanotube photoluminescence and absorption spectroscopy in high magnetic fields. Through his research with the Kono group Jonah has traveled to Humboldt University in Berlin; Laboratoire National des Champs Magnétiques Pulsés in Toulouse, France; the University of Tokyo; and the National High Magnetic Field Laboratories in Tallahassee, FL and Los Alamos, NM to conduct collaborative research on high magnetic field spectroscopy of single walled carbon nanotubes.

Junichiro Kono, born in 1966, received his B.S. and M.S. degrees in applied physics from the University of Tokyo in 1990 and 1992, respectively, and completed his Ph.D. in physics from the State University of New York at Buffalo in 1995. He was a postdoctoral research associate in condensed matter physics at the University of California, Santa Barbara in 1995–1997 and the W. W. Hansen Experimental Physics Laboratory Fellow in the Department of Physics at Stanford University in 1997–2000. He joined the Department of Electrical and Computer Engineering of Rice University in 2000 as an Assistant Professor and was promoted to Associate Professor in 2005. Professor Kono's current research interests include optical studies of low-dimensional systems; spintronics and quantum information processing; nonlinear, ultrafast, and quantum optics in solids; phenomena in ultrahigh magnetic fields; and terahertz phenomena in semiconductors. He has given more than 120 invited conference talks, colloquia, and seminars and published more than 140 papers as well as 9 book chapters and review articles.

References

[1] Y. Arakawa and H. Sakaki, App. Phys. Lett. **40**, 939 (1982).
[2] T. Ogawa and T. Takagahara, Phys. Rev. B **43**, 14325 (1991).
[3] T. Ogawa and T. Takagahara, Phys. Rev. B **44**, 8138 (1991).
[4] R. Loudon, Am. J. Phys. **27**, 649 (1959).
[5] R. J. Elliot and R. Loudon, J. Phys. Chem. Solids **8**, 382 (1959).
[6] R. J. Elliot and R. Loudon, J. Phys. Chem. Solids **15**, 196 (1960).
[7] W. Wegscheider et al., Phys. Rev. Lett. **71**, 4071 (1993).
[8] R. Ambigapathy et al., Phys. Rev. Lett. **78**, 3579 (1997).
[9] H. Akiyama, L. N. Pfeiffer, A. Pinczuk, K. W. West, and M. Yoshita, Solid State Commun. **122**, 169 (2002).
[10] D. S. Citrin, Phys. Rev. Lett. **69**, 3393 (1992).
[11] H. Akiyama et al., Phys. Rev. Lett. **72**, 924 (1994).
[12] R. Saito, G. Dresselhaus, and M. S. Dresselhaus, Physical Properties of Carbon Nanotubes (Imperial College Press, London, 1998).
[13] M. S. Dresselhaus, G. Dresselhaus, and Ph. Avouris (eds.), Carbon Nanotubes: Synthesis, Structure, Properties, and Applications, Topics in Applied Physics No. 18 (Springer, Berlin, 2001).
[14] S. Iijima, Nature (London) **354**, 56 (1991).
[15] M. J. O'Connell et al., Science **297**, 593 (2002).
[16] http://www.nanotube.org/.
[17] http://www.nanotubeoptics.com/.
[18] S. M. Bachilo et al., Science **298**, 2361 (2002).
[19] R. B. Weisman and S. M. Bachilo, Nano Lett. **3**, 1235 (2003).
[20] Y. Miyauchi, S. Chiashi, Y. Murakami, Y. Hayashida, and S. Maruyama, Chem. Phys. Lett. **387**, 198 (2004).
[21] J. Lefebvre, Y. Homma, and P. Finnie, Phys. Rev. Lett. **90**, 217401 (2003).
[22] G. N. Ostojic et al., Phys. Rev. Lett. **92**, 117402 (2004).
[23] L. Huang, H. N. Pedrosa, and T. D. Krauss, Phys. Rev. Lett. **93**, 017403 (2004).
[24] F. Wang, G. Dukovic, L. E. Brus, and T. F. Heinz, Phys. Rev. Lett. **92**, 177402 (2004).
[25] Y.-Z. Ma et al., J. Chem. Phys. **120**, 3368 (2004).
[26] G. N. Ostojic et al., Phys. Rev. Lett. **94**, 097401 (2005).
[27] S. G. Chou et al., Phys. Rev. B **72**, 195415 (2005).
[28] A. Hagen et al., Phys. Rev. Lett. **95**, 197401 (2005).
[29] Y. S. Lim et al., Nano Lett. **6**, 2696 (2006).
[30] A. Hartschuh, H. N. Pedrosa, L. Novotny, and T. D. Krauss, Science **301**, 1354 (2003).
[31] H. Htoon, M. J. O'Connell, P. J. Cox, S. K. Doorn, and V. I. Klimov, Phys. Rev. Lett. **93**, 027401 (2004).
[32] J. Lefebvre, J. M. Fraser, P. Finnie, and Y. Homma, Phys. Rev. B **69**, 075403 (2004).
[33] J. Lefebvre, P. Finnie, and Y. Homma, Phys. Rev. B **70**, 045419 (2004).
[34] J. Chen et al., Science **310**, 1171 (2005).
[35] S. Zaric et al., Science **304**, 1129 (2004).
[36] S. Zaric et al., Nano Lett. **4**, 2219 (2004).
[37] S. Zaric et al., Phys. Rev. Lett. **96**, 016406 (2006).
[38] I. B. Mortimer and R. J. Nicholas, Phys. Rev. Lett **98**, 027404 (2007).
[39] J. Shaver et al., Nano Lett. **7**, 1851 (2007).
[40] M. S. Arnold, S. I. Stupp, and M. C. Hersam, Nano. Lett. **5**, 713 (2005).
[41] M. S. Arnold, A. A. Green, J. F. Hulvat, S. I. Stupp, and M. C. Hersam, Nature Nanotechnology **1**, 60 (2006).
[42] J. A. Fagan, et al., unpublished.
[43] F. Wang, G. Dukovic, E. Knoesel, L. E. Brus, and T. F. Heinz, Phys. Rev. B **70**, 241403(R) (2004).
[44] Y.-Z. Ma, L. Valkunas, S. L. Dexheimer, S. M. Bachilo, and G. R. Fleming, Phys. Rev. Lett. **94**, 157402 (2005).
[45] L. Huang and T. D. Krauss, Phys. Rev. Lett. **96**, 057407 (2006).
[46] Ph. Avouris, J. Chen, M. Freitag, V. Perebeinos, and J. C. Tsang, Phys. Stat. Solid. B **243**, 3197 (2006).
[47] F. Wang et al., Phys. Rev. Lett. **98**, 047402 (2007).
[48] J. Crochet, M. Clemens, and T. Hertel, J. Am. Chem. Soc., in press.
[49] Z. Zhu et al., J. Phys. Chem. C **111**, 3831 (2007).
[50] V. Perebeinos, J. Tersoff, and Ph. Avouris, Phys. Rev. Lett. **92**, 257402 (2004).
[51] H. Zhao and S. Mazumdar, Phys. Rev. Lett. **93**, 157402 (2004).
[52] V. Perebeinos, J. Tersoff, and Ph. Avouris, Nano Lett. **5**, 2495 (2005).
[53] C. D. Spataru, S. Ismail-Beigi, R. B. Capaz, and S. G. Louie, Phys. Rev. Lett. **95**, 247402 (2005).
[54] E. Chang, D. Prezzi, A. Ruini, and E. Molinari, cond-matt/0603085 .
[55] T. Ando, J. Phys. Soc. Jpn. **66**, 1066 (1997).
[56] T. G. Pedersen, Phys. Rev. B **67**, 073401 (2003).
[57] C. L. Kane and E. J. Mele, Phys. Rev. Lett. **90**, 207401 (2003).
[58] T. G. Pederson, Carbon **42**, 1007 (2004).
[59] E. Chang, G. Bussi, A. Ruini, and E. Molinari, Phys. Rev. Lett. **92**, 196401 (2004).
[60] C. D. Spataru, S. Ismail-Beigi, L. X. Benedict, and S. G. Louie, Phys. Rev. Lett. **92**, 077402 (2004).
[61] F. Wang, G. Dukovic, L. E. Brus, and T. F. Heinz, Science **308**, 838 (2005).
[62] J. Maultzsch et al., Phys. Rev. B **72**, 241402 (2005).
[63] J. González, F. Guinea, and M. A. H. Vozmediano, Phys. Rev. B **59**, R2474 (1999).
[64] C. L. Kane and E. J. Mele, Phys. Rev. Lett. **93**, 197402 (2004).
[65] J. W. Mintmire and C. T. White, Phys. Rev. Lett. **81**, 2506 (1998).
[66] H. Ajiki and T. Ando, J. Phys. Soc. Jpn. **62**, 1255 (1993).
[67] H. Ajiki and T. Ando, Physica B **201**, 349 (1994).
[68] S. Roche, G. Dresselhaus, M. S. Dresselhaus, and R. Saito, Phys. Rev. B **62**, 16092 (2000).
[69] J. Kono and S. Roche, Magnetic properties, in: Carbon Nanotubes: Properties and Applications, edited by M. J. O'Connell (CRC Press, Taylor & Francis Group, Boca Raton, 2006), Chap. 5, pp. 119–151.
[70] T. Ando, J. Phys. Soc. Jpn. **75**, 024707 (2006).
[71] P. Nikolaev et al., Chem. Phys. Lett. **313**, 91 (1999).
[72] B. Kitiyanan, W. Alvarez, J. Harwell, and D. Resasco, Chem. Phys. Lett. **317**, 497 (2000).
[73] Y. Homma, Y. Kobayashi, T. Ogino, and T. Yamashita, App. Phys. Lett. **81**, 2261 (2002).
[74] V. C. Moore et al., Nano. Lett. **3**, 1379 (2003).

[75] S. Bachilo et al., J. Am. Chem. Soc. **125**, 11186 (2003).
[76] H. Ajiki and T. Ando, J. Phys. Soc. Jpn. **62**, 2470 (1993).
[77] J. P. Lu, Phys. Rev. Lett. **74**, 1123 (1995).
[78] F. Tsui, L. Jin, and O. Zhou, Appl. Phys. Lett. **76**, 1452 (2000).
[79] D. A. Walters et al., Chem. Phys. Lett. **338**, 14 (2001).
[80] M. Fujiwara et al., J. Phys. Chem. A **105**, 4383 (2001).
[81] M. F. Islam, D. E. Milkie, C. L. Kane, A. G. Yodh, and J. M. Kikkawa, Phys. Rev. Lett. **93**, 037404 (2004).
[82] D. Karaiskaj, C. Engtrakul, T. McDonald, M. J. Heben, and A. Mascarenhas, Phys. Rev. Lett. **96**, 106805 (2006).
[83] S. Berger et al., Nano. Lett. **7**, 398 (2007).
[84] S. Kazaoui et al., Appl. Rev. Lett. **87**, 211914 (2005).
[85] Y. Miyauchi, Y. Murakami, S. Chiashi, and S. Maruyama, 27th Fullerene Nanotubes General Symposium, 2004.
[86] L.-J. Li, R. J. Nicholas, R. S. Deacon, and P. A. Shields, Phys. Rev. Lett. **93**, 156104 (2004).
[87] J. Shaver et al., Dynamic magnetic alignment of single-walled carbon nanotubes in megagauss fields, in: Narrow Gap Semiconductors 2005, Proceedings of the Twelfth International Conference on Narrow Gap Semiconductors, Toulouse, France, 3–7 July 2005, edited by J. Kono and J. Léotin (Institute of Physics, Bristol, 2005).
[88] J. R. Lakowicz, Principles of fluorescence spectroscopy, in: Methods in Materials Research (Plenum Publishing Corp., New York, 2006).
[89] J. A. Fagan et al., Phys. Rev. Lett. **98**, 147402 (2007).
[90] J. Shaver et al., unpublished.
[91] L. Cognet et al., Science **316**, 1465 (2007).

